M.A. Korzhuev

A.A. Baikov Institute of Metallurgy and Material Science of RAS,
49, Leninskiy Ave., Moscow, 119991, Russian Federation

M.A. Korzhuev

THERMOELECTRIC NANOSTRUCTURES: PROS AND CONS

The limits for increase in the figure of merit Z and power W of thermoelectric materials (TEM) at nanostructurization are determined. It is shown that parameters Z and W of nanostructures (NS) vary due to the transitions $\lambda_{ph} \rightarrow$ and $\lambda_e \rightarrow a$ in TEM. (Here, a is interatomic distance, λ_{ph} and λ_e are average mean free paths of phonons and electrons in the samples). It is found out that in the range $1 \sim \lambda_{ph}/a < \lambda_e/a < 2 – 3$ the transition $\lambda_e \rightarrow a$ can be used for a simultaneous increase in the Z and W of TEM. It is established that NS TEM with the simultaneously increased parameters Z and W can effectively work in maximum power mode in thermoelectric power converters. Some negative characteristics of NS TEM are also revealed. It is optimal carrier concentration mismatch of TEM parameters Z and W, increase in the electrical and thermal contact resistances, as well as development of diffusion instability of samples at high temperatures $T > T_T \sim 0.5\ T_m \sim 400 – 500$ K. (Here, T_T is the Tammann temperature and T_m is material melting temperature).

Key words: thermoelectricity, figure of merit *Z* and power *W*, nanostructures (NS).

Introduction

At the present time many researchers study the properties of nanosized material particles ($x \sim 10^{-9}$ m), as well as the bulk heterogeneous nanostructures (NS) formed on their basis with a small identity period $x = 1 – 100$ nm [1]. It was found that the properties of such NS can differ considerably from the properties of homogeneous crystalline materials, which is generally related to the impact of surface and (or) quantum-size effects [2]. Thus, for a series of NS thermoelectric materials (TEM) there was a considerable increase in the thermoelectric figure of merit $Z = W/\kappa$ (up to 5 times and more) and power $W = \alpha^2\sigma$ (up to 1.5 – 2 times) at room temperature (Table 1). (Here α is the Seebeck coefficient, σ and $\kappa = \kappa_L + \kappa_e$ are the electric conductivity and thermal conductivity, κ_L and κ_e are the lattice and electron components of thermal conductivity) [3-4]. The maximum figure of merit values

$$Z_{\max} \sim W_{\max}\kappa_p^{-1} \sim Nm_d^{3/2}\mu T^{3/2}e^r\kappa_p^{-1}, \quad (1)$$

are known to be achieved in TEM at temperatures $T_{\max} = E_g/bk_0$ that are determined by the onset of intrinsic conductivity development in the samples. (Here N is the number of equivalent extremums in conduction band (valence), m_d is the effective mass of the density of states in a separate extremum, $\mu = \sigma/(en(p))$ is mobility, e is elementary charge, $n(p)$ is electron (hole) concentration in the samples, T is absolute temperature, r is scattering parameter, E_g is energy gap width, k_0 is the Boltzmann constant, $b = 5 – 10$ is the coefficient that varies depending on the ratio between electron and hole mobilities $a = \mu_e/\mu_p$ in the samples) [3-4]. It is generally assumed that at the transition "crystal → NS" the band structure of TEM is not changed (N, $m_d \sim$ const) [1]. In so doing, increase in $Z_{\max}$ of NS TEM is

attributable to a decrease in κ_L and increase in r due to additional scattering of phonons and electrons (holes) on the inhomogeneities with $x = 1 – 100$ nm (Table 1) [1, 2]. Research on NS TEM is a new promising direction of modern material science. Here, alongside with the evident advantages of NS TEM, some of their essential shortcomings were revealed. Thus, increase in Z of samples is, as a rule, accompanied by a reduction of σ and W, which complicates the use of NS TEM in power thermoelectric converters (TEC) (generators (TEG), coolers (TEC), heaters (TEH)), operated in maximum power mode [1]. Moreover, NS TEM are also characterized by complexity and high cost of fabrication, toxicity and reduced reproducibility of characteristics [5]. The major fault of NS is their instability (morphological, diffusion, chemical), which becomes apparent in the process of manufacture, storage and operation of samples [1, 2]. Finally, installation of NS into TEC entails additional problems related to optimization of materials and connection of legs [1-6]. The purpose of this work was all-round analysis of the strong and weak points of NS TEM, as well as determination of the immediate prospects of their use in TEC.

1. Preparation and properties of NS TEM

1.1. Formation of PGEC phase

The bulk NS TEM were obtained by different methods that can be conventionally classified as "artificial" and "natural" (Table 1) [5-14]. In the former case the necessary identity periods x in the samples were assigned by means of additional technological operations (grinding with subsequent sintering, evaporation and epitaxial growth of nanolayers, introduction of "quantum dots", irradiation, etc.) (Table 1) [5, 7-9]. In the latter case (less expensive and promising one) the nano-like TEM structures were obtained "spontaneously" as a result of "self-organization" of initially homogeneous, nonequilibrium samples, with various phase transitions (decomposition of oversaturated solid solutions, superstructural transitions, doping and self-doping of disordered phases, etc.) (Table 1) [6, 10-14]. In all cases the researchers' immediate objective was to obtain from TEM the "phonon glass-electron crystal" phase (PGEC) (Table 1) [2]. The PGEC is a partially disordered phase of TEM which is characterized by low thermal conductivity κ_L inherent in amorphous materials, and high electric conductivity σ, typical of crystals [1, 2]. As a result, at the transition "crystal → PGEC" considerable growth of TEM parameter Z can be observed [1]. The possibility of PGEC phase formation in TEM is related to the difference in average mean free paths of phonons and electrons in crystals:

$$\lambda_{ph} = 3\kappa_{ph} / CV \tag{2}$$

and

$$\lambda_e = v\tau = \left(2E_F / m_d\right)^{1/2} m_c\mu / e = \hbar(3\pi^2 n / N^2)^{1/3}\mu / e, \tag{3}$$

where $C = C_{mol}\, d/M$ is heat capacity of volume unit, C_{mol} is molar heat capacity, d is density, M is molecular mass, V is sound velocity, v and $\tau = \tau_0 E^{r-½}$ is velocity and average in energy E relaxation time of electrons or holes, r is scattering parameter, τ_0 is energy-independent factor, E_F is the Fermi energy, e is the unit cell, μ is current carrier mobility, $N = m_d/m_c$ is the number of extremums in the band, m_c and m_d are the effective masses of conductivity and density of states of electrons (holes) in the samples [15, 16]. As a rule, for crystalline semiconductors we have: $a << \lambda_{ph} << \lambda_e$ (here $a \sim 0.3$ nm is interatomic distance) (3, Fig. 1) [16]. However, crystalline TEM were selected from semiconductor materials by Z_{max} criterion (1). Therefore, they are noted for low κ_p values and high N, which according to (1) and (2), determines low λ_{ph} and λ_e values in the samples (Fig. 1) [15-19]. Thus, TEM turn to be closer to the transitions $\lambda_{ph} \to a$ and $\lambda_e \to a$ than conventional semiconductor materials, which facilitates formation of PGEC phase in the samples [16].

Table 1

Change in the properties of crystalline samples at "artificial" and "natural" nanostructurization of TEM by different methods

NS preparation technique	"Artificial"				"Natural"			
	Introduction of "quantum dots" [7]	Evaporation of superlattices [8]	Grinding and pressing [5]	Super fast cooling and pressing [9]	Spinodal decomposition of *PbS* particle (3 – 5 nm) [10] [a]	Paraelectric phase doping (T_c > 630 – 700 K) [6] [a]		Transition into superionic phase (T> 413 K) [11-13]	Crystallization of superlattices [14]
						GeTe<5%*Bi*>	TAGS-90 [c]		
Sample	*PbTe/PbSeTe*	Bi_2Te_3/ Sb_2Te_3	$Bi_{0.3}Sb_{1.7}Te_3$	$Bi_{0.52}Sb_{1.48}Te_3$	$(PbTe)_{0.92}(PbS)_{0.08}$			$Cu_{1.99}Se$	$GeBi_4Te_7$
x, nm	10	16	10/(100-300)*	$10^4/10^3$ *	10-20	~ 1.2 [d]	~ 0.9 [d]	~ 0.6 [e]	2.4
T, K	300	300	300	300	650	800→750	800→750	700	300
$\bar{\lambda}_e/a$	9.2→8.6**	8.8→6.4**	8.8→6.2**	9.2→6.0**	10→7.5**	3→2**	3→2**	0.9**	14**
λ_{ph}/a	6.0→1.2**	3.3→1.03**	1.5→1.7**	2.5→1.7**	4.0→1.8**	3→1.1**	3→1**	1**	~1.4**
α, μV/K	-300→-330**	-250→-261**	196→213	230→250	-200→(-200)**	140→200	140→200	240	-160
σ, S/cm	300→290**	810→590**	810→580	850→550	400→(300)**	2000→750	2000→1000	190	500
κ, W/(m·K)	2.5→0.6	1.45→0.6	0.94→0.82	1.36→0.9	1.1→0.5	4..5→1.8	4..5→~2.3	1.0	0.8
W, W/(cm·K)	28→32	51→40	31→26	45→34	16→12	39→27	39→40	1.1	12.8**
$Z{\cdot}10^3$, 1/K	~1.1→5.3	~3.5→6.7	~3.1→3.2	~3.3→3.7	1.4→2.3	0.9→1.7	0.9→1.7	1.1	1.6**
PGEC phase	+	+	–	–	–	+	+	Glass	–

* – before/after pressing; ** – estimates of this work; [a] – comparison to *PbTe*; [b] – comparison to *GeTe*; [c] – $(AgSbTe_2)_{0.1}(GeTe)_{0/9}$; [d] – average distance between impurity atoms; [e] – average distance between copper atoms of melted sublattice.

As long as the transition $\lambda_{ph} \rightarrow a$ in TEM is generally terminated sooner than the transition $\lambda_e \rightarrow a$, in the range

$$a = \lambda_{ph} < \lambda_e \tag{4}$$

formation of PGEC phase appears to be possible (5, 6, Fig. 1) [16].

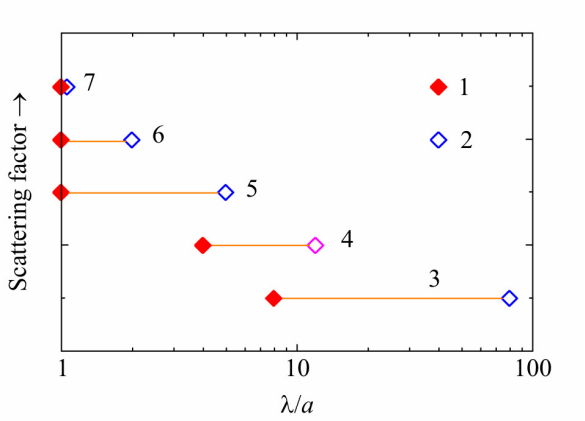

Fig. 1. Dependence of mean free path of phonons λ_{ph}/a and electrons λ_e/a (2) on scattering factor (3 – 7). Samples: 3 – solid semiconductors; 4 – 7 – TEM; 5 – 6 – PGEC phase; 7 – amorphous bodies. Materials: 4 – PbTe [1, 6]; 5 – PbTe/PbSeTe ($1 \sim \lambda_{ph}/a < \lambda_e/a$) [7]; 6 – TAGS ($1 \sim \lambda_{ph}/a < \lambda_e/a < 2 – 3$) [6, 10]; 7 – $Cu_{1.99}Se$ ($1 \sim \lambda_{ph}/a \sim \lambda_e/a$) [11-13]. Temperature, T, K: 5 – 300; 4 – 600; 6, 7 – 700.

1.2. λ-diagnostics of NS TEM

To determine belonging of samples (Table 1) to PGEC phase (3), we used the method of λ-diagnostics of TEM based on the estimation of values λ_{ph} and λ_e by the formulae (1) and (2) [16]. In the estimates, the data of original works as well as the reference data was employed [20, 21]. For *GeTe<Bi>* alloys and TAGS-90 the x parameters were calculated in the approximation of uniform distribution of dopants in the sample, and for $Cu_{1.99}Se$ alloys – of mobile interstitial copper ($T > T_c = 700$ K) (Table 1). From Table 1 it is seen that for *PbTe/PbSeTe* [7] and Bi_2Te_3/Sb_2Te_3 [8] samples the PGEC phase (3) is formed already at room temperature, as confirmed by a drastic increase in Z by a factor of 2 – 5.[1] Formation of PGEC phase (3) was also observed in doped alloys *GeTe <Bi>* and TAGS-90 [6] at a temperature of $T = 750 – 800$ K, which is accompanied by Z increase by a factor of ~ 2 as compared to *GeTe* (Table 1). The samples of $(PbTe)_{0.92}(PbS)_{0.08}$ [10] were also close to formation of PGEC phase ($Z^{650\,K}$ increase by a factor of ~ 1.6 as compared to *PbTe*) and $GeBi_4Te_7$ [14] ($Z^{300\,K}$ increase by a factor of ~ 1.6 as compared to *GeTe*) (Table 1). However, in $Bi_{0.3}Sb_{1.7}Te_3$ [5] and $Bi_{0.52}Sb_{1.48}Te_3$ [9] samples the transition $\lambda_{ph} \rightarrow a$ proved to be incomplete, PGEC phase was not obtained and, as a result, Z value increased only slightly (Table 1). The incompleteness of the transition $\lambda_{ph} \rightarrow a$ in the sample $Bi_{0.52}Sb_{1.48}Te_3$ [9] (Table 1) is due to insufficient material dispersion ($x \sim 10^3$ nm). At the same time, the sample $Bi_{0.3}Sb_{1.7}Te_3$ [5] (Table 1) obtained from nanoparticles of the necessary size ($x \sim 10$ nm, in the course of hot pressing was recrystallized with grain increase (effect of "knockout" from nanoregion) ($x = 10 \rightarrow 300$ nm) [16]. Moreover, in all NS TEM (Table 1) there was also the transition $\lambda_e \rightarrow a$ related to increased electrons (holes) scattering with dispersion of samples. In the superionic $Cu_{1.99}Se$ the two transitions $\lambda_{ph} \rightarrow a$ and $\lambda_e \rightarrow a$ were completed ($T = 700$ K), and the sample became quasi-amorphous

[1] According to [5], the results of [7, 8] have not been reproduced to this date in any other laboratory of the world, NS based devices have not been created either.

($\lambda_e \sim \lambda_{ph} \sim a$) (7, Fig. 1) [11-13]. The results of λ-diagnostics of NS TEM (Table 1) allow determination of the basic mechanisms responsible for a change in Z and W. From Table 1 it is seen that formation of PGEC phase and Z increase of NS TEM is due to a decrease in $\kappa_L \sim \lambda_{ph}$ with the transition $\lambda_{ph} \rightarrow a$. In so doing, the attendant $\lambda_e \rightarrow a$ transition, as a rule, reduces W of TEM due to reduction of $\sigma \sim \lambda_e$ (Table 1). The exception is provided by the samples of *PbTe*/*PbSeTe* [7] and TAGS-90 [6] (Table 1) where a slight growth of W was observed due to increased α of the samples. In case of NS [7] the growth of α was accounted for by additional current carrier scattering on "quantum dots" ($x = 10 – 16$ nm) [1], and for the sample [6] – by peculiarities of TEM band structure in the transient region $1 < \lambda_e/a \sim 3$ [16].

1.3. Two-channel band model of TEM

According to [15, 16], the band structure of TEM in the transient region $1 < \lambda_e/a \sim 2 – 3$ is varied considerably. With the transition $\lambda_e \rightarrow a$ in TEM in addition to a "band" conduction channel ($\lambda_e / a > 1$) (1, Fig. 2), a diffusion conduction channel is formed in conduction (valence) band (2), related to the appearance of a group of current carriers with a low mobility, moving in the sites of crystal lattice ($\lambda_e/a = 1$) [15]. With further scattering increase, the "band" current carriers disappear, and the "diffusion" ones cover the entire band (arrow, Fig. 2). The model (Fig. 2) corresponds to p-type conductivity and acoustic scattering mechanism ($r = 0$). With increase in $r > ½$, the situation is changed, namely the "diffusion" conduction channel (2, Fig. 2) is formed near the band edge, and then it is distributed in the band toward larger energies [16].

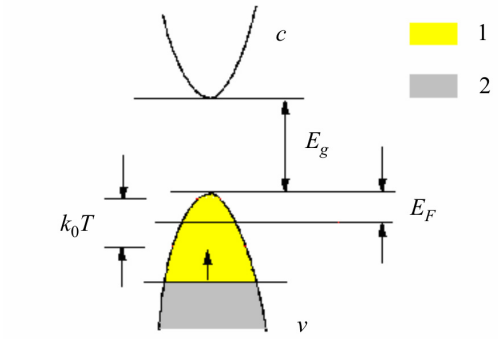

Fig. 2. Two-channel band model of TEM. Bands: v – valence; c – conduction. Channels: 1 – "band" ($\lambda_e > a$), 2 – "diffusion" ($\lambda_e = a$). The arrow shows a direction of channel boundary displacement in the energy scale with scattering increase in the samples (p-type conductivity, r = 0) [15, 16].

In the two-channel model (Fig. 2) the kinetic coefficients of samples with constant total carrier concentration ($p = p_1 + p_2 = \text{const}$) are given by the expressions $\sigma = \sigma_1 + \sigma_2$, and $\alpha = \alpha_1 \cdot t_1 + \alpha_2 \cdot t_2$ (Here, $t_i = \sigma_i/\sigma$ is transport ratio, α_i and σ_i are partial thermoEMF and electric conductivity, $i = 1, 2$ are numbers of channels with "band" ($\lambda_e > a$) and "diffusion" ($\lambda_e = a$) conduction, respectively) [16]. Fig. 3 shows the results of calculations of a relative change in thermoelectric figure of merit Z (curve 1), power W (curve 2) and thermal conductivity κ (curve 3) of TEM samples in the region of PGEC phase existence. In the calculations, use was made of the band parameters $\mu_1/\mu_2 \sim \kappa_L/\kappa_e \sim 10$ and $\kappa_L^{cryst}/\kappa_L^{PGEC} = 3$ (here, $\mu_{1,2}$ are partial mobilities, κ_L and κ_e are the lattice and electron components of thermal conductivity), as well as scattering parameters $r = 0$ (acoustic scattering) and $r = ½$ (scattering on neutral centres) for the "band" (1) and "diffusion" (2) conduction channels, respectively (Fig. 2) [16].

From Fig. 3 it follows that in the range of $1 < \lambda_e/a < 2 – 3$ the values of Z and W in TEM can increase simultaneously (curves 1 and 2). At $t_1 \sim 0.8$ maximum increase in Z by a factor of ~ 2.5 – 3 and W by a factor of 1.3 – 1.4 (curves 1 and 2, Fig. 3) is possible due to a combined effect of the transitions

$\lambda_{ph} \rightarrow a$ and $\lambda_e \rightarrow a$. The possibility of α and W growth (3, Fig. 3) in the model (Fig. 2) is related to energy selection of the "band" and "diffusion" current carriers taking part in conductivity [16]. Earlier the model (Fig. 2) was used to account for the anomalous growth of Z and W in $GeTe$ and $Cu_{1.99}Se$ alloys at a high temperature [15]. According to estimates (Fig. 3), two-channel conductivity can be also responsible for the simultaneous growth of Z and W at a high temperature ($T = 700 – 800$ K) in the nano-like structures of the type p-TAGS $((AgSbTe_2)_{1-x}(GeTe)_x)$ ($\lambda_e/a \sim 2$) (Table 1) [6, 10], as well as p-LAST-m ($AgPb_mSbTe_{2+m}$, $m = 18 – 22$) ($ZT = 1.6 – 2.2$) [10].

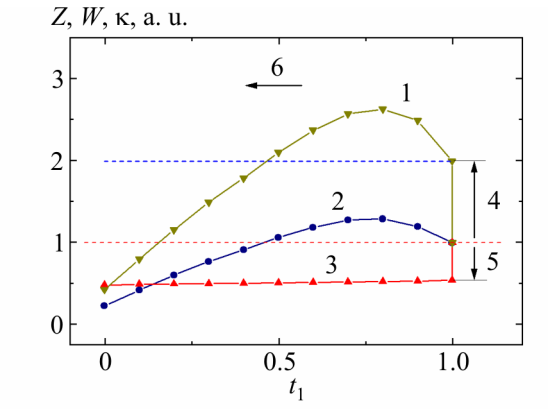

Fig. 3. Relative change in the figure of merit Z (1), power W (2) and thermal conductivity κ (3) with the transitions $\lambda_{ph} \rightarrow a$ (4, 5) and $\lambda_e \rightarrow a$ (6) in TEM depending on the transport ratio of band charge carriers t_1 (T = const).

2. Comparison of NS TEM and crystalline TEM

2.1. λ-diagnostics of crystalline TEM

The results of λ-diagnostics of crystalline TEM are given in Fig. 4 ($a – f$). Figs. 4 a and 4 b show polyterms λ_{ph}/a (a), λ_e/a (b) ($T = T_{max}$) (curves 3 and 4) depending on E_g of the best low-, medium- and high-temperature TEM [1, 6, 10-13, 21, 22]. Figs. 4 c and 4 d show the respective polyterms T_{max} (curves 5 – 8), as well as optimal charge carrier concentration $n^{opt}(p^{opt})$ (curve 9) and the Fermi energy E_F of TEM (curve 11). From Fig. 4 a and 4 b it is seen that with increase in E_g and T_{max}, the transitions $\lambda_{ph} \rightarrow a$ and $\lambda_e \rightarrow a$ occur in crystalline TEM that change the characteristics of samples. Fig. 4 c shows the impact of the transition $\lambda_e \rightarrow a$ on the T_{max} value of TEM (curves 7 and 8). According to Fig. 4 c, far from the transition $\lambda_e \rightarrow a$ ($\lambda_e/a > 10$, $E_g < 0.4$ eV) TEM behave as conventional semiconductors with high mobility μ, the values of T_{max} being in the range of $5 < b < 10$ (5 – 8, Fig. 4 c). However, at $E_g > 0.5 – 0.7$ eV and $\lambda_e / a < 2 – 3$ the values of T_{max} go beyond the range of $5 < b < 10$ (curves 7 and 8, Fig. 4 c). The effect is attributable to the appearance in the samples of "diffusion" charge carriers with a low mobility ($\lambda_e = a$), which increases the relative contribution of minor carriers to development of intrinsic conductivity in the samples ($r = 0$) [15, 16]. Here we have $T_{max}(p) < T_{max}(n)$ (curves 7 and 8, Fig. 4 c), since generally $a = \mu_e/\mu_p > 1$ [11]. The transition $\lambda_e \rightarrow a$ also affects the polyterms $n^{opt}(p)^{opt}$, $E_F = f(E_g)$ in TEM (Fig. 4 d), where one can see a reduction in growth rate $n^{opt}(p)^{opt}$ (curve 9) and even slight reduction of $E_F \sim ½\, k_0 T_{max}$ (curve 11) related to T_{max} reduction in the region of $\lambda_e \sim a$ (curve 10). Figs. 4 e and 4 f show polyterms of the figure of merit $(ZT)_{max}$ (curve 12) and power $W = f(E_g)$ (curve 15) in crystalline TEM ($T = T_{max}$). Curve 12 (Fig. 4 e) has an extended maximum $(ZT)_{max} \sim 1$ in the range of 0.1 eV $< E_g <$ 1.0 eV and drops in the area of low and high E_g. According to Figs. 4 a and 4 f, condition $(ZT)_{max} \sim 1$ in the range of

0.1 eV < E_g < 0.6 eV (curve 12, Fig. 4 *e*) is maintained due to a compensating effect of the transitions $\lambda_{ph} \rightarrow a$ and $\lambda_e \rightarrow a$ leading to a simultaneous reduction of κ_L and W of the samples.

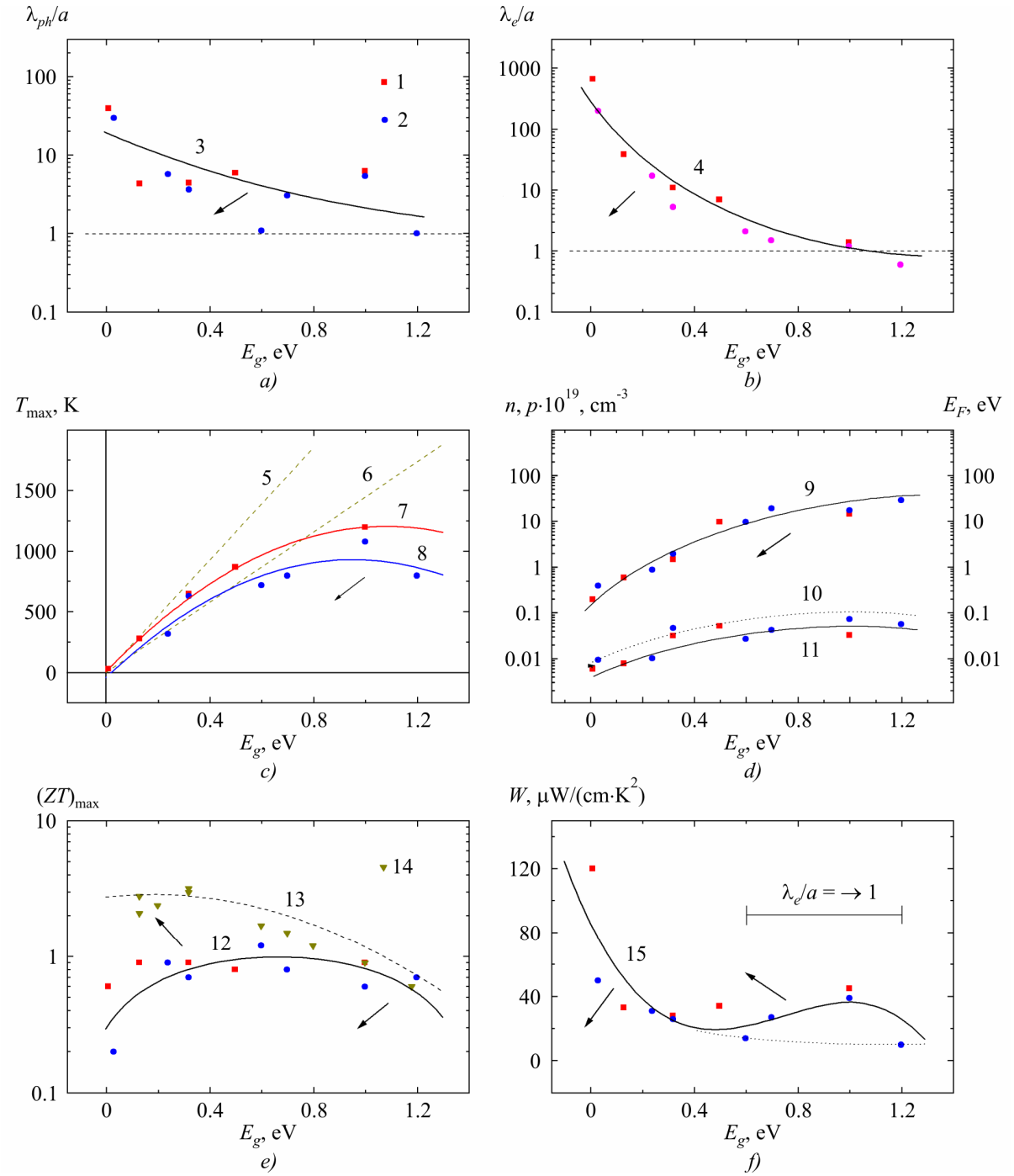

Fig. 4. Polyterms λ_{ph}/a (a), λ_e/a (b), T_{max} (c), n^{opt} (p^{opt}) and E_F (d) $(ZT)_{max}$ (e) and W (T_{max}) (f) depending on the energy gap E_g of TEM ($T = T_{max}$). Samples: 1 – 12 – crystals [1, 6, 10-13, 20-22]; 13, 14 – NS [7, 8, 10, 22]. Materials (in order of increasing E_g): 1 – n-type (BiSb, Bi_2Te_3, PbTe, $CoSb_3$, SiGe); 2 – p-type (BiSb <Sn>, Sb_2Te_3, PbTe, TAGS, GeTe, SiGe, $Cu_{1.99}Se$). 1, 2, 14-experiment; 5, 6, 10, 13 – calculation. Design formulae: 5, 6 – $E_g = bk_0T$ (b: 5 – 5; 6 – 10); 10 – $E = k_0T_{max}$; 13 – $y = (ZT_{max}$ (curve 12)) (λ_{ph}/a). Directions of possible changes in TEM characteristics at formation of NS are shown with arrows.*

In so doing, the decay in curve 12, Fig. 4 *e* at $E_g > 1.0$ eV is related to completion of the transition $\lambda_e \rightarrow a$ ($\lambda_e/a = 1$), and the decay at $E_g < 0.1$ eV – to requirements of thermodynamics – α,

$W \to 0$, at $T \to 0$, [1, 4, 6]. The results obtained (Fig. 4) show that the mechanisms of Z and W increase in NS and crystalline TEM at a high temperature are of the same physical nature. In so doing, the difference in the characteristics of NS TEM and crystalline TEM at T = const is due to different stages of the transitions $\lambda_{ph} \to a$ and $\lambda_e \to a$ in the samples. Hence it follows that the expected characteristics of NS TEM can be estimated based on the properties of crystalline TEM by extrapolation $\lambda_{ph} \to a$ and $\lambda_e \to a$. Directions of possible changes in the characteristics of TEM at the transition "crystal → PGEC" are shown by arrows in Fig. 4.

2.2. The "crystal-PGEC" transition

According to Fig. 4, on condition of E_g = const, the "crystal → PGEC" transition in TEM results in the reduction of λ_{ph} and λ_e, T_{max}, n^{opt} (p^{opt}), E_F, as well as W (at $E_g < 0.4$ eV). In so doing, for any values of E_g the value of ZT is increased due to a reduction of NS κ_L (curves 12 → 13, Fig. 4 *e*). Curve 13, Fig. 4 *e* gives the upper limit of ZT increase in samples when passing to PGEC phase. Curve 13, Fig. 4 *e* was calculated for NS by formula (1) based on curve 12 for crystals on condition of $\lambda_{ph}/a = 1$ (Fig. 4 *e)*. From Fig. 4 *e* it is seen that the greatest ZT increase when passing to PGEC phase (up to ~ 10) can be expected only at $T_{max} < 600$ K and $E_g < 0.4$ eV (curve 12 → 13). With $T_{max} > 600$ K and $E_g > 0.4$ eV the possibilities of ZT increase for NS in PGEC phase are reduced considerably (up to~ 1.5) (Fig. 4 *e)*.[2] By and large, the above conclusion is confirmed by the experimental observations of $(ZT)_{max}$ for NS TEM (14, Fig. 4 *e*). Further increase in $(ZT)_{max}$ of NS TEM can be promoted by increase in power parameter W with the transition $\lambda_e/a \to 1$ related to a displacement of W features in the range of $1 < \lambda_e/a < 3$ toward low E_g (Fig. 4 *e*).

2.3. Simultaneous increase in *Z* and *W* of TEM

The main problem of using NS TEM in TEC is a reduction in the majority of cases of power parameter W of NS as compared to crystalline materials (Table 1) [1, 2]. As is known, the Z value of TEM determines maximum temperature difference of TEC and TEH, namely $\Delta T_{max} = ½\, ZT_1^2 = ½\, Z((1 + 2T_0Z)^{½} - 1)/Z)^2$ and TEC efficiency – $\eta = \eta_c\ (M_0 - 1)/(M_0 + T_c/T_h)$ (maximum efficiency mode), or $\eta = \eta_c/(2 + 4/ZT_h - \eta_c/2)$ (maximum power mode) (Here, $\eta_c = (T_0 + T_1)/T_1$ is the Carnot factor, $M = R/r$ is the relative electric load of TEG; R is the electric resistance of load; $M_0 = (1 + Z\,\overline{T})^{1/2}$; $\overline{T} = ½\ (T_0 + T_1)$ is the average temperature) [1]. On the other hand, the W of TEM determines maximum cooling capacity of TEC and TEH, namely $Q_{max} = \Delta T_{max}\kappa S/l \sim ½ W\, T_1^2$, as well as maximum net power of TEG $W_{max} = W\Delta T^2/4 = WS/4l$ [1, 6]. As an example, Fig. 5 shows a relative change in the temperature difference $\Delta T/\Delta T_0$ of TEC with different Z and W as a function of cooling capacity Q/Q_0. From Fig. 5 it is evident that using NS TEM with increased Z (curves

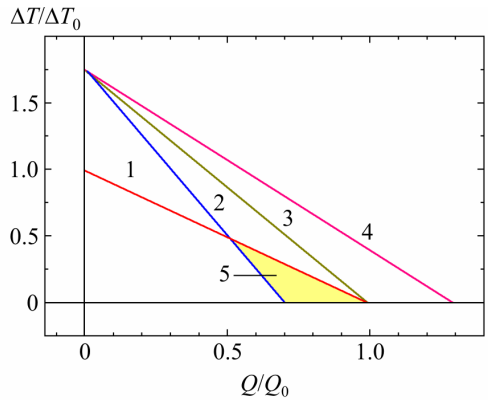

Fig. 5. Relative change in temperature difference $\Delta T/\Delta T_0$ (1 – 4) versus cooling capacity Q/Q_0 of TEC. Materials: 1 – crystals ($\Delta T/\Delta T_0 = Q/Q_0 = 1$); 2 – 4 – NS. $Z_{HS}/Z_{CR} = 3$; W_{HS}/W_{CR} : 2 – 0.7; 3 – 1; 4 – 1.3. 5 – region where NS (2) are inferior in characteristics to crystals (1).

[2] This conclusion refers to averaged Z values of TEM. For instance, in *SiGe* alloys, where $\lambda_{ph}/a \sim 8$ (Fig. 4 *a*), there are considerable additional reserves for Z growth [1].

2 – 4), in the mode of zero thermal load ($Q = 0$) one can always expect ΔT_{max} growth as compared to crystals (curve 1). However, when passing to maximum power mode, with increase in Q in Fig. 5 appears a region (5), with NS characteristics inferior to crystals. Hence it follows that for an adequate use of NS TEM in TEC a simultaneous increase in parameters Z and W is needed (1 → 3, 4, Fig. 5) [1, 10, 20]. For a simultaneous increase of Z and W in TEM the most efficient method was optimization of the band parameters of materials (N, E_F and energy gap E_g). It is also possible to use quantum-size effects (superlattices, quantum wells, wires and dots, etc.), to create in the permitted band close to E_F the "resonance" states, to use grain boundary scattering providing carriers "filtration" according to energies (growth of r and α) [1, 4, 6, 8, 10]. According to Fig. 3 – 4, for a simultaneous increase of Z and W in NS TEM one can also use the effect of "two-channel" conduction acting in TEM in the range of $1 \sim \lambda_{ph}/a < \lambda_e/a < 2 – 3$. If necessary, further increase of Z and W in TEM is possible due to the use of quantum effects in NS [1, 10, 20].

3. Other problems of using NS TEM

3.1. NS TEM instability

Different types of NS TEM instability are directly related to the instability of nanoparticles that form them and possess increased surface energy [1, 2, 23]. Therefore, in the process of compaction of such nanoparticles when preparing the bulk materials there is recrystallization of grains accompanied by increase in their size by several orders (effect of "knockout" from the nanoregion) (Table 1) [5]. However, in some cases the "knockout" effect can be conquered, for instance, by using plasma sintering of particles accompanied by formation of secondary grain substructure [1, 10, 22]. The main type of NS TEM instability is their diffusion instability manifested in the rise of temperature $T > T_T \sim 0.4 – 0.6\ T_m \sim 400 – 700$ K (Here, T_T and T_m are the Tammann and material melting temperatures, respectively) [22]. Fig.6 shows melting temperature T_m (1), T_{max} (2) and the Tammann temperature $T_T = 0.6\ T_m$ (3) of crystalline TEM depending on E_g of samples.

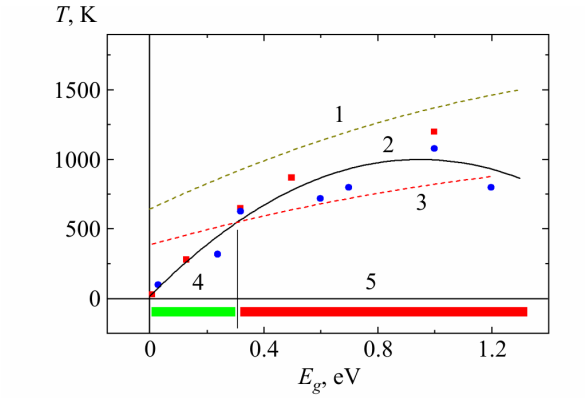

Fig. 6. Melting temperature T_m (1), T_{max} (2) and the Tammann temperature $T_T = 0.6\ T_m$ (3) of crystalline TEM versus the energy gap E_g. 4 and 5 are NS stability and instability ranges at $T = T_{max}$. Samples: see caption to Fig. 4.

From Fig. 6 it is seen that at $T_{max} > 500 – 600$ K and $E_g > 0.3$ eV NS TEM are instable at temperature $T \sim T_{max}$ (range 5). At temperature T_{max} only the alloys with $T_{max} < 500$ K and $E_g < 0.3$ remain stable (range 4), which restricts considerably the prospects of using NS in high-temperature region. To the full extent this conclusion refers to "artificial" NS TEM and to a lesser degree to NS TEM obtained at decomposition of oversaturated solid solutions (Table 1). Even to a lesser extent this conclusion is related to natural superlattices of TEM obtained by crystallization from the melt [1], as

well as strongly disordered nano-like structures of the type $Ge_{1-x}Te$, TAGS, LAST and $Cu_{2-x}Se$ (Table 1). Diffusion instability of NS TEM directly accounts for their chemical instability determined by high rate of reagents diffusion along the grain boundaries. Various technical methods for combatting chemical instability of NS TEM are applied with profit [1, 22].

3.2. Change in material optimization parameters

The transition "crystal → NS" reduces the values of T_{max}, n^{opt} (p^{opt}), and in some cases E_F of the samples (Fig. 4). This necessitates a change in optimization rules of NS TEM as compared to crystals. Fig. 7 demonstrates the Bergholz diagrams qualitatively explaining the differences in the optimal concentration of current carriers in crystal and NS [3]. From Fig. 7 it is seen that on condition of $\alpha \sim \alpha$ (crystal) $\sim \alpha$ (HS) $\sim$ const (Table 1), the optimal concentration of current carriers n_{opt} of NS will be reduced, and the known mismatch between n_{opt} for Z and W will increase ($\Delta_1 > \Delta_2$).

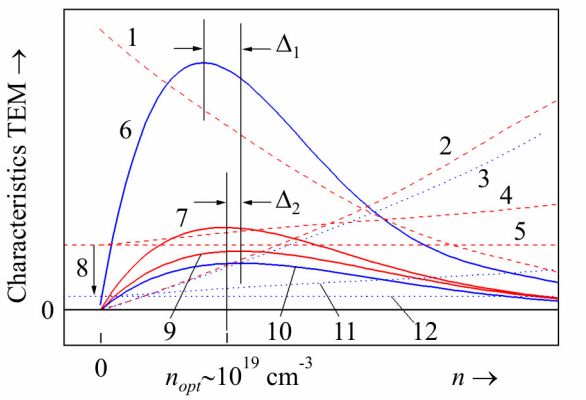

Fig. 7. The Bergholz diagrams of TEM. 1, 2, 4, 5, 7, 9 – crystals; 1, 3, 6, 10, 11, 12 – NS (T = 300 K). Characteristics: 1 – α ~ α (crystal) ~ α (HS) ~ const; 2, 3 – σ; 4, 11 – κ = κ_L + κ_e; 5, 12 – κ_L; 6, 7 – Z; 9, 10 – W. Mismatch in n_{opt} between Z and W: Δ_1 are NS; Δ_2 are crystals. 8 is transition λ_{ph}→a.

The mismatch $\Delta_1 > \Delta_2$ can result in the necessity of developing NS TEM with different parameters as applied to maximum efficiency and maximum power modes of TEC.

3.3. Contact effects and material saving

The transition "crystal → NS" is accompanied by increase in thermal ($r^T = \kappa^{-1}$) and electrical resistance ($\rho = \sigma^{-1}$) of the samples. As a result, the use of NS TEM in TEC is accompanied by increase in transient contact thermal and electrical resistances of thermocouples, which can generate a need for longer legs and reduced device efficiency [1, 6]. However, in [23] it was shown that for the case of automobile thermoelectric generators (ATEG) using gas heat carriers [6] the contribution of contact resistances of NS TEM can be assumed to be inessential as compared to parasitic resistances of heat exchangers. In this case, the use of NS TEM can lead to a simultaneous increase in TEC efficiency and considerable saving of costly TEM (up 3 times and more) [24]. However, in the case of TEC using liquid and solid heat carriers, the contribution of NS contact resistances to TEC efficiency can prove to be essential, and it should be taken into account in the development of devices [6].

Conclusion

Research on NS TEM is a new upcoming trend of modern material science [1, 2]. In this paper, a thorough analysis of NS TEM characteristics is made and mechanisms for improving their

thermoelectric figure of merit Z and power W are determined. Transition of TEM into "phonon glass-electron crystal" (PGEC) phase underlies the growth of NS parameter Z. The possibility of PGEC phase formation in the samples ($a = \lambda_{ph} < \lambda_e$) is related to the proximity of TEM to the transitions $\lambda_{ph} \rightarrow a$ and $\lambda_e \rightarrow a$. (Here a is interatomic distance, λ_{ph} and λ_e is the average mean free path of phonons and electrons). To determine the degree of proximity to PGEC phase, the method of λ-diagnostics of TEM based on the estimation of λ_{ph} and λ_e values in the samples is developed in [16]. The use of λ-diagnostics allowed to establish that increase of Z and W in NS TEM, as well as TEM crystals at high temperature are determined by the same mechanisms. Owing to this result, the theoretical limits of increase in Z and W parameters in NS TEM were estimated in various temperature ranges. According to estimates, the greatest growth of Z in NS TEM is possible at room and lower temperatures; with a rise in temperature, the possibilities of Z growth in NS TEM are reduced. The use of λ-diagnostics also allowed establishing the mechanisms responsible for growth of Z and W in NS TEM. It is shown that formation of PGEC phase and growth of Z in NS TEM is due to reduction of $\kappa_L \sim \lambda_{ph}$ at the transition $\lambda_{ph} \rightarrow a$. In so doing, the attendant transition $\lambda_e \rightarrow a$, as a rule, reduces W of TEM due to reduction of $\sigma \sim \lambda_e$. As long as reduction of W complicates the use of NS TEM in power TEC, it is necessary to further increase α and W of NS TEM by various methods. With this aim in view, in the present paper it is proposed to use the effect of two-channel conduction assuring simultaneous growth of Z and W in the range of $1 \sim \lambda_{ph}/a < \lambda_e/a < 2 - 3$. This paper also covers some negative characteristics of NS TEM preventing their wide use in TEC. In particular, the ranges of diffusion instability of NS at high temperatures are determined. It is shown that at present the "safe" range of using "artificial" NS TEM is probably restricted to near-room and lower temperatures. One is inclined to think that the above disadvantages of NS TEM can be overcome, and the stability of samples at high temperatures can be increased using various technical methods. However, since the above problems have not been solved up to now, only the "natural" NS such as naturally-occurring superlattices based on multicomponent systems seem to be the most promising so far for high-temperature use[3]. Also of great interest are "natural" nano-like structures of the type *GeTe*, TAGS and LAST based on strongly disordered phases, that have already proved their reliability by failure-free operation on space objects for 10 and more years [1, 6, 10].

References

1. G.S. Nolas, J. Sharp, and H.J. Goldsmid, *Thermoelectrics. Basic Principles and New Materials Developments* (Berlin: Springer, 2001), 293 p.
2. G. Slack, *New Materials and Performance Limits for Thermoelectric Cooling*, CRC Handbook of Thermoelectrics, Ed.: D.M. Rowe (N.Y.: Boca Raton, 1995), P. 407 – 440.
3. U. Birkholz, Thermoelectric Elements, In: *Amorphous and Polycrystalline Semiconductors*. Ed. by W. Heywang. Transl from German (Moscow, Mir, 1987), P. 47 – 74.
4. L.I. Anatychuk, *Thermoelements and Thermoelectric Devices* (Kyiv: Naukova Dumka, 1979), 768 p.
5. L.P. Bulat, D.A. Pshenai-Severin, I.A. Drabkin, et al., Mechanisms for Thermoelectric Figure of Merit Improvement in the Bulk Nanotructured Polycrystals, *J. Thermoelectricity* **1**, 13 – 18 (2011).
6. A.S. Okhotin, A.A. Yefremov, V.S. Okhotin, and A.S. Pushkarsky, *Thermoelectric Generators* (Moscow: Atomizdat, 1976), 320 p.

[3] The "natural" NS also include layered crystals of the type Bi_2Te_3 whose identity period $x \sim 3$ nm appears somewhat lower than that optimal for TEM ($x \sim 10 - 40$ nm) [1, 2].

7. T.C. Harman, P.J. Taylor, M.P. Walsh, and B.E. LaForge, Quantum Dot Superlattice Thermoelectric Materials and Devices, *Science* **297**, 2229 (2002).
8. R. Ventkatasubramanian, E. Siivola, T. Colpitts, and B. O'Quinn, Thin-Film Thermoelectric Devices with High Room-Temperature Figures of Merit, *Nature* **413** (6856), 597 – 602 (2001).
9. L.D. Ivanova, L.I. Petrova, Yu.V. Granatkina, V.S. Zemskov, S.A. Varlamov, A.S. Ivanov, Yu.P. Prilepo, A.M. Sychev, A.G. Chuiko, Materials Based bon $Bi_{0.5}Sb_{1.5}Te_3$ Solid Solution Prepared with the Use of Spinning Method, Thermoelectrics and Their Applications. Ed. by M.V. Vedernikov, L.N. Lukyanova (The Petersburg Nuclear Physics Institute RAS, 2010), P. 88 – 93.
10. J. Sootsman, D.Y. Chung, and M.G. Kanatzidis, New and Old Concept in Thermoelectric Materials *Angew. Chem. Int. Ed.* **48**, 8616 – 8639 (2009).
11. A.A. Voskanyan, P.N. Inglizyan, Ya.M. Shevchenko, and T.B. Shmakova, Thermal Field Effect on the Electric Properties of Copper Selenide, *Semiconductors* **14** (4), 804 – 806 (1980).
12. M.A. Korzhuev, V.F. Bankina, B.F. Gruzinov, and G.S. Bushmarina, Electrophysical Properties of Superionic $Cu_{2-x}Se$, *Semiconductors* **23** (9), 1545 – 1551 (1989).
13. M.A. Korzhuev, V.F. Bankina, B.A. Yefimova, and N.N. Filipovich, Electrophysical Properties of $Cu_{2-x}Se$ Alloys Doped with Electroactive Dopants, *Semiconductors* **24** (5), 805 – 812 (1990).
14. V.S. Zemskov, L.E. Shelimova, O.G. Karpinsky et al., Thermoelectric Materials Based on Layered Compounds in Chalcogenide Systems with Homologous Series, *J. Thermoelectricity* **1**, 15 – 29 (2010).
15. M.A. Korzhuev, A.V. Laptev, and V.F. Degtyarev, The Use of Two-Channel Conductivity Model for the Description of Kinetic Coefficients of $Ge_{1-x}Te$ и $Cu_{2-x}Se$ Type Crystals in High Temperature Region, *Thermoelectrics and Their Applications* (The Petersburg Nuclear Physics Institute, 2002), P. 133 – 138.
16. M.A. Korzhuev, Effect of Average Mean Free Path of Phonons and Electrons on the Parameters of Figure of Merit Z and Power W of Thermoelectric Nanostructures, *Thermoelectrics and Their Applications*, Ed. by M.I. Fedorov, L.N. Lukyanova (The Petersburg Nuclear Physics Institute, 2002), P. 99 – 105.
17. M.A. Korzhuev, Concomitant Effects in High-Performance Thermoelectric Materials, *Vysokochistye Veschestva* **2**, 74 – 89 (1996).
18. M.A. Korzhuev, Symmetry Analysis of Thermoelectric Energy Converters with Inhomogeneous Legs, *JEMS* **39** (9), 1381 – 1385 (2010).
19. M.A. Korzhuev, The Hall Effect in Thermoelectric Materials of the Type $Ge_{1-x}Te$ and $Cu_{2-x}Se$ in the Region $\lambda \rightarrow a$, *Physics of the Solid State* **35** (11), 3043 – 3052 (1993).
20. *Physicochemical Properties of Semiconductor Substances*. Handbook. Ed. by A.V. Novoselova (Moscow: Nauka, 1979), 340 p.
21. N.N. Kiseleva, V.A. Dudarev, and M.A. Korzhuev, The Bandgap of Solids (Semiconductors, Dielectrics, Semimetals). Determination of the Bandgap of Inorganic Substances-Semiconductors, *Datebase «Bandgap» b.g.imet-db.ru/ about database.asp. 2007.*
22. T. Kajikawa, Advances in Thermoelectric Power Generation Technology in Japan, *J. Thermoelectricity* **3**, 5 – 18 (2011).
23. K. Meyer, *Physicochemical Crystallography*. Transl. from German. (Noscow: Metallurgiya, 1972), 480 p.
24. M.A. Korzhuev, Yu.V. Granatkina, Some Bottlenecks in the Vehicular Thermoelectric Generators and a Search for New Materials to Eliminate Them, *J. Thermoelectricity* **1**, 74 – 86 (2012).

Submitted 22.04.2013.